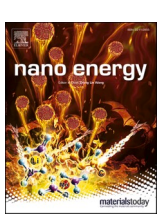
ELSEVIER

Contents lists available at ScienceDirect

Nano Energy

journal homepage: www.elsevier.com/locate/nanoen





Standalone stretchable RF systems based on asymmetric 3D microstrip antennas with on-body wireless communication and energy harvesting

Senhao Zhang ^{a,b,c,1}, Jia Zhu ^{c,*,1}, Yingying Zhang ^b, Zhensheng Chen ^d, Chaoyun Song ^e, Jiuqiang Li ^{a,b}, Ning Yi ^c, Donghai Qiu ^b, Kai Guo ^{a,b}, Cheng Zhang ^f, Taisong Pan ^g, Yuan Lin ^g, Honglei Zhou ^h, Hao Long ⁱ, Hongbo Yang ^{a,b,**}, Huanyu Cheng ^{c,*}

- a School of Biomedical Engineering (Suzhou), Division of Life Sciences and Medicine, University of Science and Technology of China, Hefei 230022, PR China
- ^b Suzhou Institute of Biomedical Engineering and Technology, Chinese Academy of Science, Suzhou 215011, PR China
- ^c Department of Engineering Science and Mechanics, The Pennsylvania State University, University Park, PA 16802, USA
- d Department of Electrical Engineering (ESAT), KU Leuven, Leuven 3001, Belgium
- ^e School of Engineering and Physical Sciences, Heriot-Watt University, Edinburgh EH14 4AS, UK
- f College of Material and Chemical Engineering, Minijang University, Fuzhou 350108, PR China
- g School of Material and Energy, University of Electronic Science and Technology of China, Chengdu 610054, PR China
- ^h Institute of Flexible Electronics Technology of THU, Jiaxing 314000, PR China
- ⁱ School of Electronic and Information Engineer, Soochow University, Suzhou 215000, PR China

ARTICLE INFO

Keywords: Stretchable microstrip antennas Mechanical assembly 3D structures On-body wireless communication RF energy harvesting Wearable and bio-integrated electronics

ABSTRACT

As an indispensable component, the stretchable antenna with the potential use in wireless communication and radio frequency (RF) energy harvesting can provide future wearable electronics with a low profile and integrated functions. However, mechanical deformations applied to stretchable antennas often lead to a shift of their resonant frequency (i.e., the detuning effect), which limits their applications to strain sensing. In addition, the on-body radiation efficiency of stretchable antennas severely degrades due to lossy human tissues. In this work, we introduce stretchable microstrip antennas with varying 3D configurations for excellent on-body radiation performance. Compared to their 2D counterpart, the stretchable 3D microstrip antennas showcase a strain insensitive resonance, improved stretchability, and enhanced peak gain. In particular, the optimized peak gain from the stretchable asymmetric 3D microstrip antenna allows it to wirelessly transmit the energy and data at an almost doubled distance, as well as a doubled charging rate from the harvested RF energy. More importantly, the integration of stretchable antenna and rectenna with stretchable sensing and energy storage units can yield a standalone stretchable RF system for future health monitoring of humans and structures. The results from this work can also pave the way for the development of self-powered units with wireless transmission capabilities for stretchable body area networks and smart internet-of-things.

1. Introduction

The development of standalone wearable biodevices hinges on wireless technology for data communication and powering [1–3], which can eliminate conventional power sources [4] and electrical wires [5] for reduced footprint and extended applications [6–10]. As the key component in wireless technology, antennas need to be stretchable to follow large human motions or natural skin deformations [11]. Early developments of stretchable or reconfigurable antennas explore

intrinsically stretchable conductive composites or liquid metals [12,13]. However, their complex fabrication processes are challenging to scale up for mass production [14] and their low conductivity often leads to a higher ohmic loss for compromised performance compared with conventional metals [15]. More importantly, the resonant frequency of these stretchable antennas significantly decreases as they are stretched (i.e., the detuning effect) [16], which limits their applications in strain sensing [17–19]. It is also challenging to integrate them with commercial off-the-shelf chips. As a result, high-performance stretchable

^{*} Corresponding authors.

^{**} Corresponding author at: Suzhou Institute of Biomedical Engineering and Technology (Sibet), Chinese Academy of Science, Suzhou 215011, PR China. *E-mail addresses*: jmz5364@psu.edu (J. Zhu), yanghb@sibet.ac.cn (H. Yang), Huanyu.Cheng@psu.edu (H. Cheng).

 $^{^{1}}$ These authors contributed equally to this work.

antennas with strain-insensitive resonance frequency are in high demand for wireless communication [20–22] and powering [23–25].

Another important consideration for stretchable antennas to be used on the body is the effect from the lossy human tissues [26,27], which drastically degrade the radiation performance to result in low on-body radiation efficiency. Compared with the bow-tie or dipole antennas [28–30] that do not have a ground plane, the antennas with a ground plane such as microstrip patch antennas [31–33] are less affected by the lossy tissues, manifested by a negligibly small change of S_{11} curves and radiation patterns. They also correspond to a low specific absorption rate (SAR), which is important for wearable RF applications. However, the meshed ground plane in the structure-engineering stretchable microstrip patch antenna leads to a relatively large back lobe in radiation patterns and degraded on-body performance [34,35]. Therefore, it is important to optimize the peak gain of the proposed stretchable microstrip antennas for wearable applications.

Previous research indicates that using a low-dielectric substrate in microstrip antennas helps to improve the peak gain [36–38]. Another research demonstrates the gain of microstrip antennas with partial substrate removal is determined by the removal location [39]. Considering that the introduction of 3D structures modifies the dielectric constant, it is reasonable to expect an improved gain for the stretchable 3D microstrip antenna. Therefore, it is worthwhile to explore stretchable 3D double-arched microstrip antennas with different configurations by mechanical assembly [40] to improve the peak gain or wireless

communication and RF energy harvesting performance. As Fig. 1 shows, after characterizing the radiation pattern to determine the optimized configuration, the stretchable 3D microstrip patch antenna is explored to demonstrate obvious improvements in wireless on-body data communication and RF energy harvesting, manifested by a doubled working distance and doubled charging efficiency, compared with their 2D counterpart. Besides wireless energy transmission for powering, the 3D stretchable microstrip patch antenna can also be combined with a flexible rectifier to harvest the radiofrequency (RF) energy for powering low-power wearable electronics, including flexible supercapacitors, stretchable strain sensors based on laser-induced graphene (LIG), on-chip temperature sensors, and Bluetooth modules. In a proof-of-concept demonstration, self-powered strain sensing has been used in body movement detection and continuous pulse monitoring, which hold potential for personal healthcare and human-machine interface. Considering the ubiquitous RF energy in the ambient environment, the harvested energy provides a complementary yet always-on energy source that is less affected by the movements or weather conditions. The stretchable 3D antennas and the resulting integrated systems with enhanced on-body performance provide a new class of microwave RF devices and stretchable standalone systems.



Fig. 1. Design concepts of the standalone stretchable RF systems based on asymmetric 3D microstrip antennas with excellent on-body wireless communication and energy harvesting.

2. Results and discussion

2.1. Stretchable 3D microstrip antennas with symmetric or asymmetric configurations

The fabrication of stretchable 3D microstrip antennas starts with the patterning of a meshed patch and a meshed ground with a UV laser (power: 0.4 μJ and speed: 2000 mm s $^{-1}$) (Fig. 2a). The 2D rectangular lattice in the meshed patch and ground consists of periodic serpentine horseshoe units with a linewidth of 100 μm (inner and outer radii of 250 μm and 350 μm) and arch angle of 180°, corresponding to a filling ratio of 25.7% (Fig. 2b). Varying the linewidth can easily yield different filling ratios, with a lower value for enhanced stretchability and a higher value for a lower radiation loss. The 3D patch is then created by the mechanical assembly with the meshed patch selectively attached to a

pre-strained (10% or 20%) elastomeric substrate (Ecoflex00–30) and then followed by the release of the pre-strain. By selecting the location of the bonding site, the double-arched structure with different 3D morphologies can be formed in the meshed patch (Fig. 2c). The 3D double-arched patches can be symmetric ("Sym_1:1") or asymmetric ("Asy_1:2") or in terms of the relative width of the two arches (with fixed overall width). As for the meshed ground plane, its full bonding to the pre-strained substrate forms a slightly wrinkled structure after the release of the pre-strain, which can easily interface with human tissues (see Experimental Section for details). The strain distribution obtained from finite element analysis (FEA) indicates a maximal principal strain of 1.02% over ½ of the cross-sectional area in all three 3D meshed patches (Fig. 2d), which is well below the fracture limit of copper. The inset feeding technique has also been adopted to excite the microstrip antenna for easy integration with other device components and facile interfacing

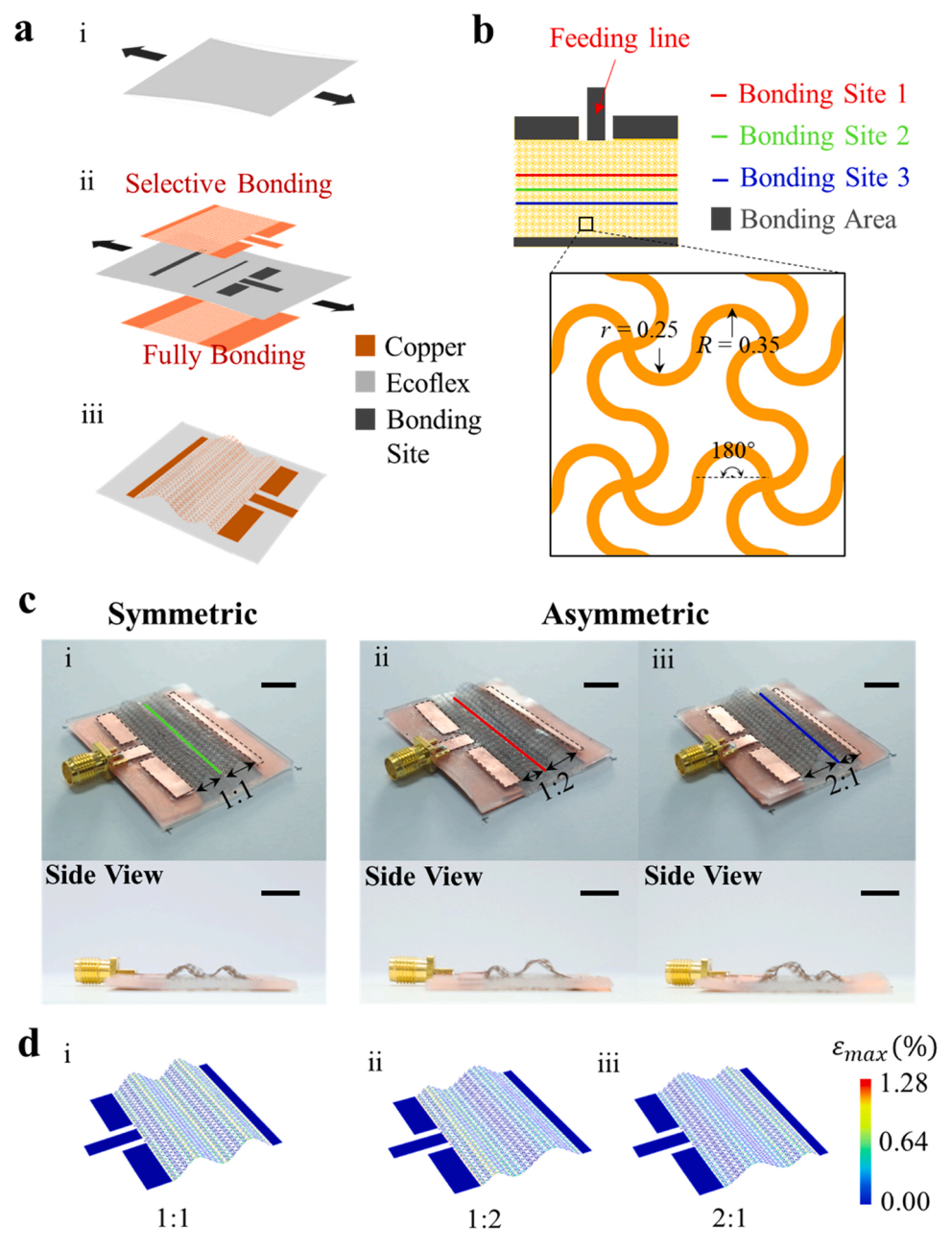


Fig. 2. Stretchable symmetric or asymmetric double-arched microstrip antennas. (a) Fabrication of double-arched microstrip antennas composed of a meshed ground and an arched meshed patch by the mechanical assembly. (b) Structures of the 2D meshed patch. Optical images (c) and simulated strain distribution (d) of the symmetric (i 1:1) and asymmetric (ii and iii, 1:2 and 2:1) double-arched microstrip antenna induced by a 10% pre-strain (scale bar, 10 mm).

with the human body. It is also worth noting that the design of the stretchable 3D antenna starts from an unstretchable solid microstrip antenna resonating at ~ 3.2 GHz (Fig. S1). Converting the solid patch and ground into meshed structures without modifying overall dimensions (Fig. S2) reduces the resonance frequency to ~ 2.5 GHz due to the increased electric length (Fig. S3). Therefore, it is important to design the initial solid microstrip antenna at a higher frequency before rendering a stretchable counterpart at the desired resonant frequency.

2.2. Mechanical-electromagnetic properties of 3D double-arched microstrip antennas

The maximum arch height is proportional to the width between adjacent bonding sites. Therefore, the maximum arch height in the symmetric double-arched patch is between those of the two arches in the asymmetric double-arched patch. The maximum arch heights measured in the experiment also validate the predictions obtained by the FEA simulation with an error of less than 4.3% (e.g., 2.15 mm in the measurement vs. 2.10 mm in the simulation for the symmetric one) (Table S1). The maximum arch height decreases with the applied strain before the arches are flattened (when the applied strain equals the prestrain) for all three 3D microstrip antennas (Fig. 3a). The changes in the morphology of the 3D structures result in the coupled mechanical-

electromagnetic properties of the three 3D microstrip antennas, which are measured by a custom-built setup (Fig. S4) and compared to their 2D counterpart. Without stretching, all three 3D microstrip antennas exhibit a resonant frequency in the 2.4-2.5 GHz range, which is smaller than that of their 2D counterpart with the meshed patch and meshed ground. This is attributed to the increased thickness of the effective dielectric layer with an air gap on top of the substrate between the patch and ground. As the tensile strain is applied, the double-arched microstrip antenna follows "ordered unraveling" to first flatten the 3D patch to the 2D meshed structure and then unfold the serpentine horseshoe units. As a result, the stretchability (\sim 20%) of the 3D microstrip antenna is approximately the sum of the level of the pre-strain (10%) and the stretchability of its 2D counterpart ($\sim 10\%$). The measured S_{11} curves of all three 3D microstrip antennas first shift to the high frequency (blueshift) in the first stage before the applied strain reaches the pre-strain, which is then followed by a shift to the low frequency (redshift). The blueshift in the 1st stage results from the increased effective dielectric constant from the reduced air gap between the arched patch and substrate (Fig. S5), whereas the redshift in the 2nd stage can be explained by the increased length of the patch as in previous studies [31,34]. In contrast, their 2D counterpart shows a decreased resonant frequency as the tensile strain is increased. As a result, the wide operational band can be maintained in the 3D microstrip antennas even upon stretching. It is

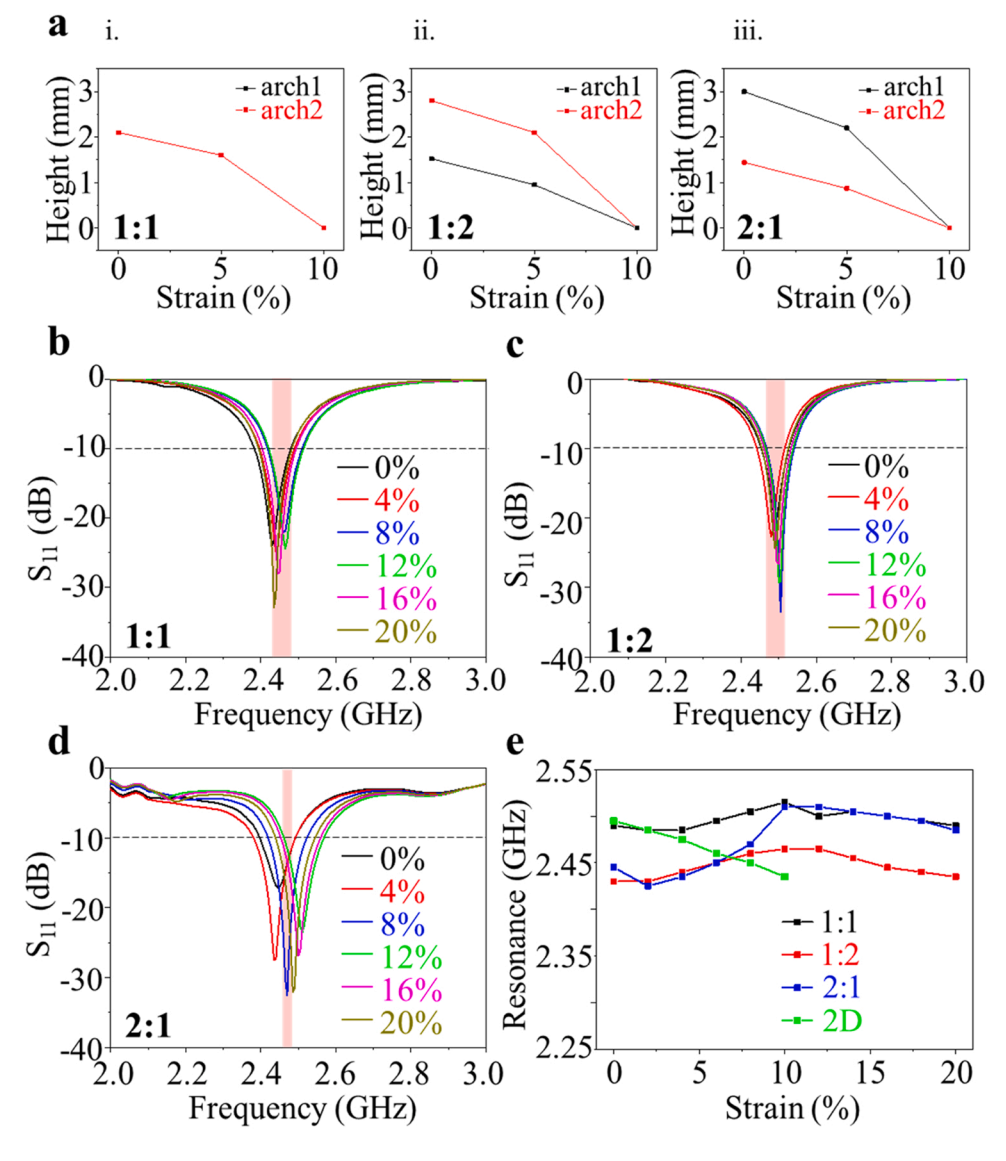


Fig. 3. Mechanical-electromagnetic properties of symmetric and asymmetric double-arched microstrip antennas induced by a 10% prestrain. (a) The arch height as a function of the applied tensile strain. S_{11} curves of symmetric (b, 1:1) and asymmetric (c and d, 1:2 and 2:1) double-arched microstrip antennas upon strain from 0% to 20%. The highlight region indicates the operational band defined by the frequency range with S_{11} values less than - 10 dB. (e) The measured resonance frequency as a function of the applied tensile strain from 0% to 20%.

also important to note that the "Asy_2:1" microstrip antenna shows a shift of 0.085 GHz in the resonance frequency upon stretching of 20%, which is much larger than that of 0.04 GHz (or 0.03 GHz) from the "Sym_1:1" (or "Asy_1:2") microstrip antenna. Because of the small shift in the resonance frequency, a large operational band of 0.060 (or 0.055) GHz over 20% stretching is obtained for the "Sym_1:1" (or "Asy_1:2") microstrip antenna. In comparison, the "Asy_2:1" microstrip antenna only shows an operational band of 0.015 GHz, indicating a less stable mechanical-electromagnetic property. However, it is still better than the stretchable single-arched microstrip antenna that can only be used for strain sensing due to frequency detuning upon stretching (Fig. S6a, d). Further increasing the number of arches from 2 to 3 with an additional

selective bonding site results in a triple-arched patch in the hierarchically structured stretchable antenna. The reduced changes in dielectric constant and dielectric layer thickness upon stretching of 20% lead to a slightly smaller variation of 0.03 GHz in resonance frequency (Fig. S6b, d) compared with 0.04 GHz for the symmetrical double-arch microstrip antenna. However, the measured radiation pattern of the triple-arched microstrip antenna exhibits a significantly lower value in the peak gain ($-0.38~\mathrm{dBm}$) (Fig. S6c), limiting its applications in on-body wireless communication and RF energy harvesting. Therefore, the double-arched antenna with an asymmetric structure (i.e., "Asy 1:2") is chosen in the following study for its strain-insensitive performance and optimized peak gain unless otherwise specified. The

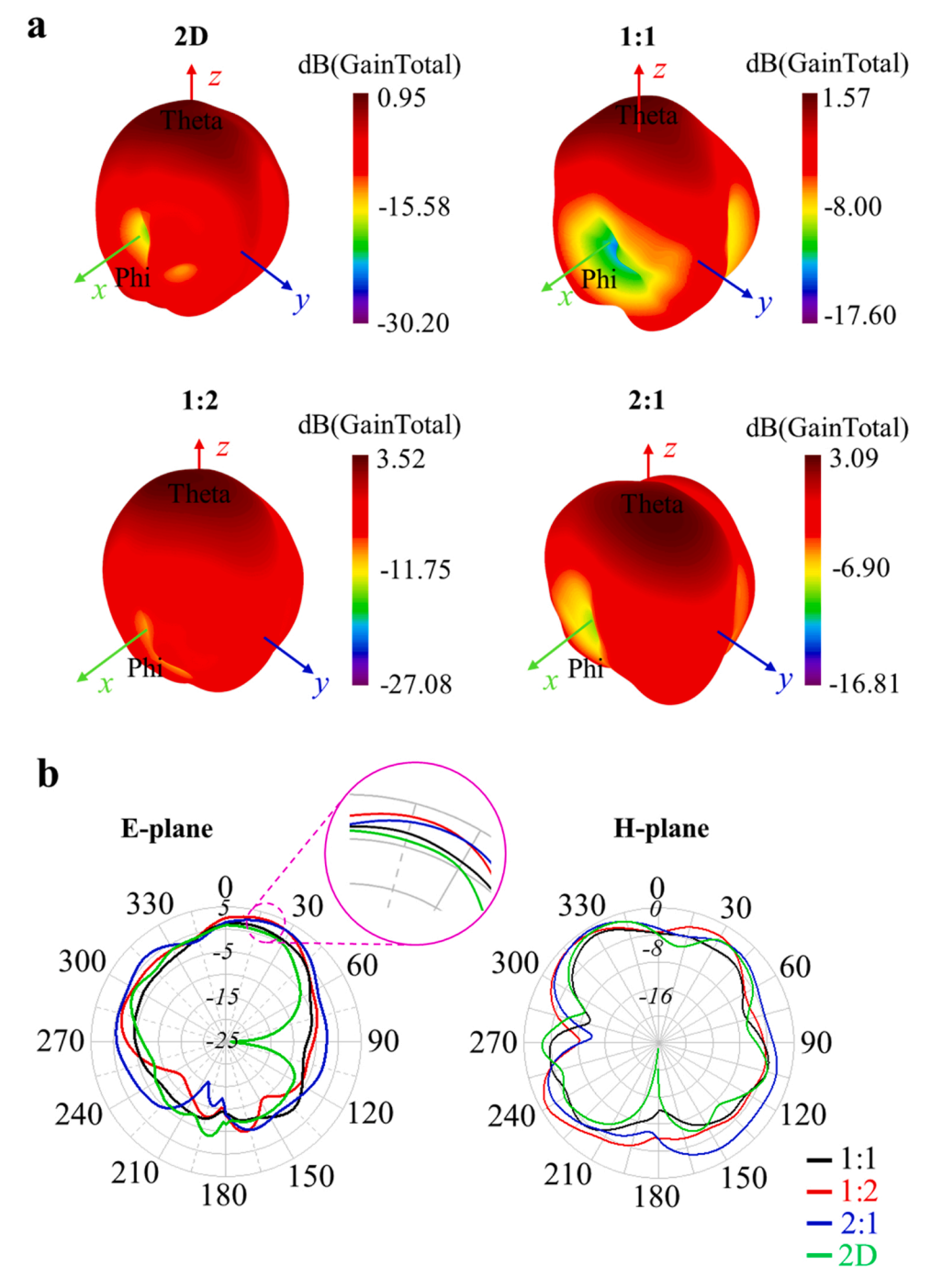


Fig. 4. Measured radiation patterns of symmetric and asymmetric double-arched microstrip antennas induced by a 10% pre-strain. (a) Measured 3D radiation patterns of symmetric and asymmetric double-arched microstrip antennas with different arch combinations and their 2D counterpart. (b) The radiation pattern on E-plane and H-plane of symmetric, asymmetric double-arched microstrip antennas and its 2D planar counterpart.

mechanical-electromagnetic property of the "Asy 1:2" double-arched microstrip antenna also remains robust and stable against cyclic stretching (Fig. S7a, b) and mechanical pressing (Fig. S7c, d). In particular, only negligible changes (less than 1%) are observed in the S₁₁ curve and resonance frequency after both types of cyclic loading over 250 times. Furthermore, the deformed 3D arch structure upon pressure loading can quickly recover to the original state after the pressure is removed (Fig. S8a and Movie S1). The variation in the S₁₁ curves is also very small even as the applied external force is increased from 0 to 20 N (Fig. S8b). The mechanical robustness of the 3D structure can be further enhanced against other potential damages by placing it inside an Ecoflex cavity without changing its S₁₁ curve (Fig. S8c, d). As discussed above, the increase in the pre-strain level can enhance the stretchability of the 3D microstrip antenna. For instance, a stretchability of 30% can be obtained in all three 3D microstrip antennas when a 20% pre-strain is applied in the mechanical assembly process (Fig. S9). However, the coupled mechanical-electromagnetic property is also affected to result in a smaller operation band (e.g., 0.025 GHz from 20% pre-strain compared with 0.055 GHz from 10% pre-strain for the "Asy 1:2" microstrip antenna). Therefore, the pre-strain level of 10% is used in the following studies unless otherwise specified.

Supplementary material related to this article can be found online at.

2.3. Radiation patterns of 3D microstrip antennas

Though the ground plane in the microstrip antenna can help isolate the lossy human tissues [41] to avoid performance degradation, the leakage of the electromagnetic field from the meshed ground in stretchable microstrip antennas causes radiation loss. In fact, the measured peak gain of 0.95 dB from the stretchable 2D meshed microstrip antenna is much smaller than that of 4.5 dB from its solid counterpart. Besides the increased stretchability and strain-insensitive resonance, the stretchable 3D microstrip antennas can also provide improved gain for improved on-body performance due to the additional air gap. Compared with the peak gain of 1.57 dB from the symmetric 3D microstrip antenna ("Sym_1:1"), the asymmetric ("Asy_1:2" and "Asy_2:1") 3D microstrip antennas further exhibit improved peak gain of 3.59 and 3.09 dB (Fig. 4a). Since a low-dielectric substrate [34-36] and partial substrate removal [37] can help improve the peak gain of microstrip antennas, the asymmetric design likely combines these two mechanisms to result in an enhanced peak gain [38,42,43]. The curvature and the relative location of these 3D structures may possibly affect the radiation performance of this new class of 3D stretchable microstrip antennas, which will be systematically investigated in future studies. The measured 3D radiation patterns of all three 3D microstrip antennas also indicate the preferred radiation along the +z direction, as the other typical microstrip antennas working in the TM10 mode [44]. The 2D radiation patterns in the E_plane and H_plane further reveal the almost unidirectional radiation on the x-y plane from all three 3D microstrip antennas and confirm the preferred radiation along the +z direction. As the tensile strain of 20% is applied, the peak gain from all three 3D microstrip antennas increases. Compared with a nearly 50% increase from 1.57 to 2.34 dB for the "Sym_1:1" antenna, the peak gain increase of 9% (from 3.52 to 3.83) and 20% (from 3.09 to 3.72) is smaller for the "Asy_1:2" and "Asy_2:1" microstrip antennas (Fig. S10). The increased peak gain possibly arises from the densified meshed networks upon stretching, which is consistent with previously reported results [34,45].

2.4. On-body wireless communication performance of 3D microstrip antennas

The 3D microstrip antennas with strain-insensitive resonance, improved stretchability, and enhanced peak gain are highly promising for use in on-body wireless communication and RF energy harvesting. With a thin adhesive Silbione layer applied on the ground to form a strong bonding to the Ecoflex substrate, the stretchable 3D microstrip

antenna can be facilely attached to the hierarchical surface of human skin on the forearm (Fig. 5a). Compared with the in-air performance, the S₁₁ curves of the 3D "Sym_1:1" and "Asy_1:2" microstrip antennas and their 2D counterpart on human arms only have a negligibly small change (Fig. 5b), which implies excellent on-body performance. Therefore, these microstrip antennas on human arms still resonate in the range from 2.40 to 2.50 GHz, corresponding to the widely used wireless communication band (i.e., 2.40-2.48 GHz for Zigbee, Bluetooth, and Wi-Fi). The wireless communication of the microstrip antennas can be conveniently carried out by using a wireless communication system consisting of two CC2538 evaluation modules (Fig. S11). One module is connected to the on-body microstrip antenna ("Sym_1:1", "Asy_1:2" and "2D counterpart") as the transmitter and the other one is connected to a nearly omnidirectional on-board inverted F antenna as the receiver. The transmitter is programmed to transmit RF energy at -3 dBm (0.50 mW). By placing the receiver from the transmitter at different distances in an open space of a university campus, the received power is then measured by the receiving board with a sensitivity of - 100 dBm (Fig. 5a).

Because of the enhanced gain in the 3D microstrip antennas compared to their 2D counterpart, they exhibit improved wireless communication performance such as higher received RF energy at the same distance over a large distance range (Fig. 5c). The higher peak gain of 3.52 dB along the +z direction from the "Asy_1:2" microstrip antenna than that of 1.57 dB from the "Sym_1:1" microstrip antenna also explains the larger received power from the former (Fig. 5d). At a representative distance of 1 m, the received powers from the "Asy_1:2" and "Sym_1:1" double-arched microstrip antennas of 29.6 \pm 3.51 and 12.3 \pm 2.08 dBm are significantly higher than that of -50.3 ± 1.15 dBm from their 2D counterpart. The enhanced wireless communication capability of the "Asy_1:2" microstrip antenna also ensures a large working distance of ~ 120 m between the transmitter and receiver, which is much farther than that of $\sim 90 \text{ m}$ from the "Sym_1:1" microstrip antenna and of \sim 80 m from the 2D counterpart. When the receiver is placed at different deflection angles from the transmitter (distance fixed at 5 m), the received power exhibits the preferred radiation along the +z direction, which is consistent with the measured radiation pattern (Fig. S12a).

Besides wireless transmission of energy for future wireless powering of stretchable device systems, the stretchable 3D microstrip antenna can also be applied for wireless transmission of data. Different from efficiency in wireless transmission of energy, data quality is of high importance in wireless communication of data. Therefore, the packet loss rate is chosen in this study as an effective parameter to evaluate the transmitted data quality. Defined as the number ratio of the lost data packets to the total sent data packets, the packet loss rate is preferred to be small or vanishing for high-quality data transmission. In this study, the transmitter is configured with the highest throughput ($\sim 1000,000$ packets) and fastest rate (~100 packets/s) to emulate the heavy network traffic. No loss of wireless transmission data (i.e., a packet loss rate of 0%) is observed in both 3D and 2D microstrip antennas for short communication distance (Fig. 5e). However, the packet loss rate from the two 3D microstrip antennas is much lower than that from their 2D counterpart as the distance increases to be over 40 m. Therefore, the effective communication distance with no data loss from the "Asy_1:2" microstrip antenna is ~ 80 m, which is much longer than that of ~ 60 m from the "Sym_1:1" microstrip antenna or of $\sim 40\,m$ from their 2D counterpart. These results confirm the significantly improved on-body wireless communication performance of the 3D asymmetric microstrip antenna. The wireless communication performance of the stretchable microstrip antenna is also minimally affected by the deformation induced by arm bending (Fig. S12), which is attributed to the straininsensitive resonance and excellent on-body performance. Besides the on-body measurements for wearable electronics, the wireless communication performance of the 3D microstrip antenna in free space has also been investigated for potential use in other stretchable device systems

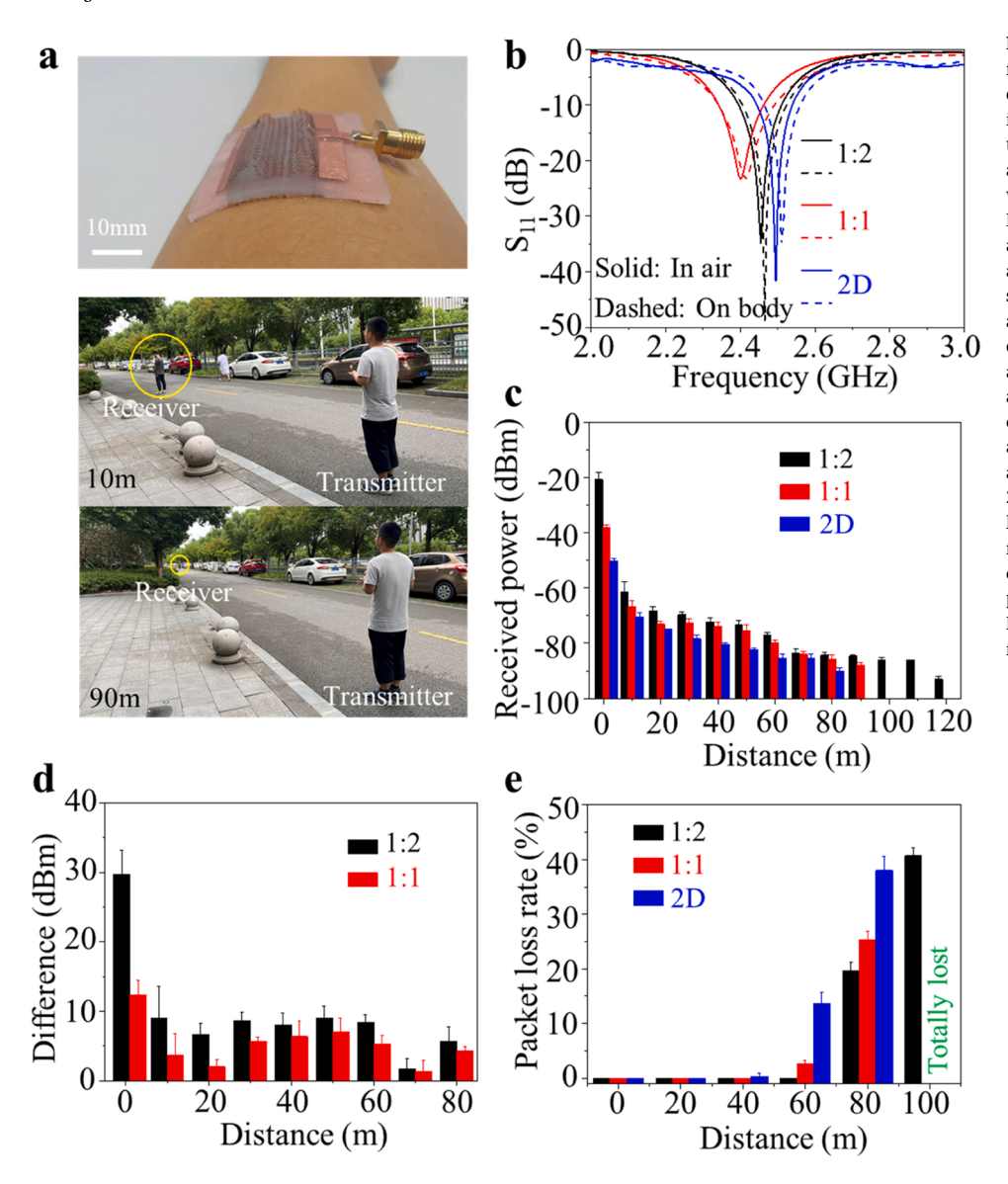


Fig. 5. Wireless on-body communication performance of symmetric and asymmetric double-arched microstrip antennas. (a) Optical images of the double-arched microstrip antenna (1:2) conformally attached to the human arm and the experimental setup to evaluate the wireless communication performance. (b) Measured S_{11} curves of the symmetric (1:1), asymmetric (1:2) double-arched microstrip antenna and its 2D planar counterpart in freespace and on a subject's arm. (c) Measured average receiving power by a receiver at different distances from the symmetric (1:1), asymmetric (1:2) double-arched microstrip antenna, and its 2D planar counterpart placed on a subject's arm. (d) The difference of average receiving power from the symmetric, asymmetric double-arched microstrip and its 2D planar counterpart. (e) Measured packet loss rates of a receiver at different distances from the symmetric (1:1), asymmetric (1:2) double-arched microstrip antenna, and its 2D planar counterpart placed on a subject's arm. Error bars calculated based on measurements from three individual tests in (c-e).

(Fig. S12e, f). Compared with the "Sym_1:1" 3D microstrip antenna in free space, the "Asy_1:2" 3D microstrip antenna still exhibits improved wireless communication performance such as higher received power and lower packet loss rate for the same operation distance. At a representative distance of 60 m, the "Asy_1:2" microstrip antenna shows a received power of -76.3 ± 1.53 dBm and a package loss rate of 0, whereas the "Sym_1:1" microstrip antenna only gives -80.7 ± 1.53 dBm and $13\pm2\%$, respectively.

2.5. On-body RF energy harvesting performance of 3D microstrip

Integrating the stretchable microstrip antenna with a rectifying circuit that has an embedded matching network conveniently yields a rectenna to harvest RF energies (Fig. 6a and Fig. S13a). The RF source with a power of 7 dBm (5.02 mW) from the evaluation board is used to evaluate the energy harvesting performance of the resulting rectenna. Because of its low activation power (~ -19 dBm), the energy management chip (AEM 30940, e-peas) is also chosen to power electronics or charge energy storage devices (detailed pin configuration and diagram shown in Fig. S13b, c). Besides directly charging an energy storage unit (e.g., batteries and capacitors), the energy management chip can also

convert the harvested RF energy into a regulated yet tunable voltage from 1.5 to 3.3 V for powering various external devices such as stretchable sensors or light emitted devices (LEDs).

The on-body energy harvesting performance of the integrated rectenna is first evaluated by using the harvested RF energy to charge a capacitor. The distance between the transmitter and rectenna is fixed at 20 mm to ensure sufficient input RF energy (above the activation threshold) and easy comparison. This distance can be much larger when a higher RF power is used. The higher input power also results in a higher RF energy harvesting efficiency in the rectifying circuit (Fig. S14). It should be noted that spin diodes in the rectifier can also be explored to significantly improve the working distance or to efficiently harvest ultralow ambient RF energies. The open voltage of the capacitor with a capacitance (C) of 680 μ F is expressed as $U = \int I(t)dt/C$, where I(t) is the charging current. Therefore, as the charging time increases, the open voltage of the capacitor increases until it reaches a saturated value of ~ 2.7 V for both 3D and 2D microstrip antennas, which indicates stable RF harvesting (Fig. 6b, c). Compared with the full charging time of 115 s from their 2D counterpart, the 3D microstrip antennas give a much faster charging, with a full charging time reduced to 57 s and 75 s for the rectenna with the "Asy 1:2" and "Sym 1:1" microstrip antennas. Considering the stored energy in the capacitor as

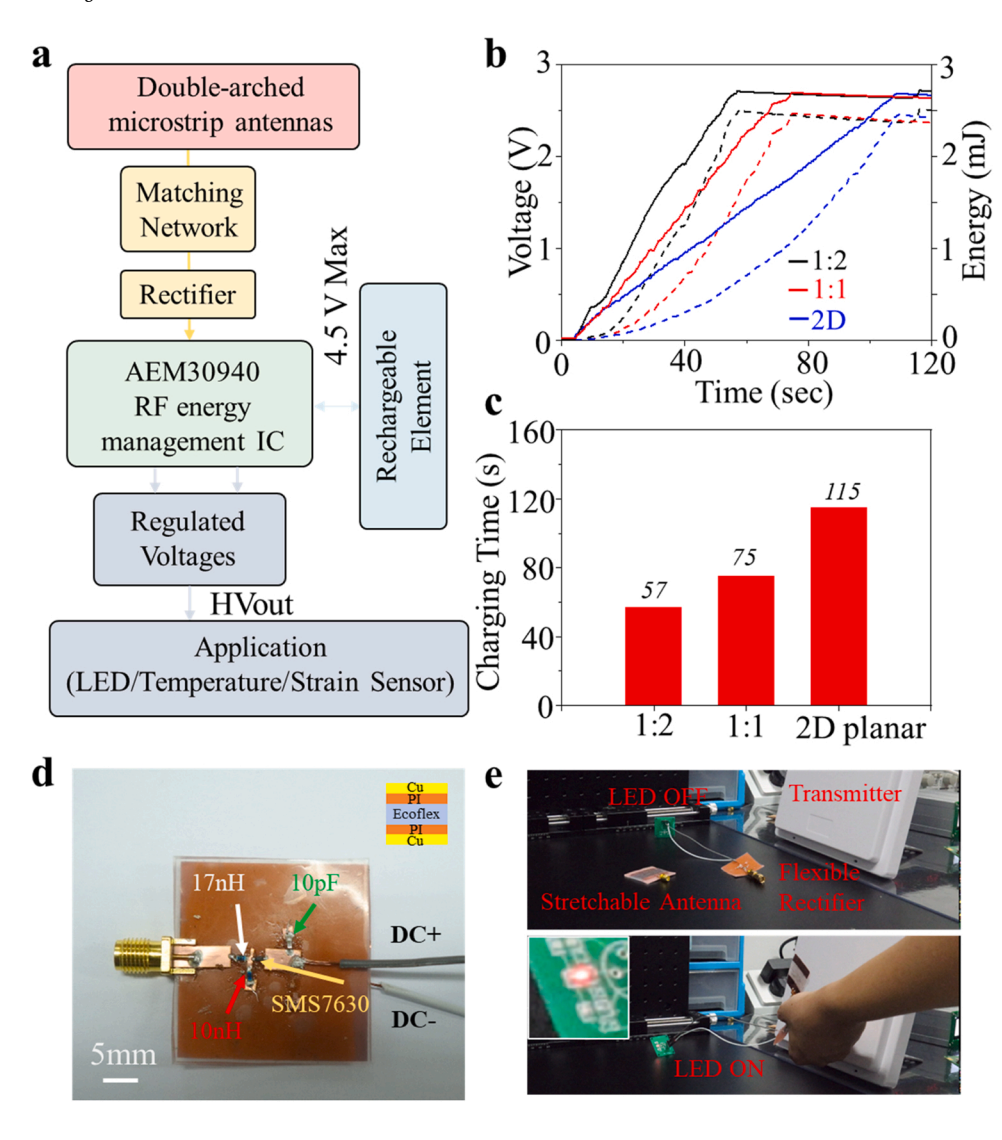


Fig. 6. Demonstration of RF energy harvesting by the integrated stretchable rectennas. (a) Schematic block diagram of the RF energy harvesting module. (b) Measured open voltage (black) and stored energy (red) of a capacitor charged by the integrated rectenna based on the stretchable 2D and 3D ("Sym_1:1" and "Asy_1:2") microstrip antenna as a function of time, with the full charging time in (c). (d) Optical image of the flexible rectifier (scale bar, 5 mm). (e) Photographs showing the LED integrated with the stretchable rectenna consisting of a stretchable antenna and flexible rectifier before (top) and after (bottom) turning on the ambient RF energy harvesting.

 $E=CU^2/2$, the average charging power from the rectenna with the "Asy_1:2" and "Sym_1:1" microstrip antenna are 43 and 33 μ J/s, which are significantly higher than that of 22 μ J/s from their 2D counterpart.

The enhanced on-body RF energy harvesting performance from the 3D rectennas is also attributed to their high peak gain. The input power received by the integrated rectenna from the RF source can be estimated by the following equation according to the Fries Transfer Formula [46]:

$$P_{input} = P_t + G_t + G_r + Lbf + L_c, (1)$$

where P_t is the transmitted RF power, G_t and G_r are the peak gain of the antenna in the transmitter and rectenna, Lbf is the free space loss between the transmitter and rectenna, and L_c is the loss of the cable. The same experimental setup implies the unchanged P_t , G_t , L_c , and Lbf for the 3D and 2D rectennas. Therefore, the input power received by the rectenna solely depends on the peak gain of the 3D (or 2D) microstrip antenna. As a result, the "Asy_1:2" microstrip antenna with the highest peak gain provides the resulting integrated rectenna with significantly improved on-body energy harvesting performance. The results confirm the importance of the asymmetric 3D structures in the 3D antennas/rectennas for excellent on-body performance.

2.6. Integrated standalone stretchable RF systems

Though the rectifier that mediates the RF-DC conversion is a vital

component in the stretchable RF system, the conventional rectifiers have been limited on rigid substrates such as Rogers Laminate PCB and FR-4, resulting in challenges for wearable applications. To address this challenge, this work designs and demonstrates a flexible rectifier on the soft Ecoflex substrate (Fig. 6d). The Schottky diode SMS7630 (Skyworks Solutions Inc.) is configured in a full-wave rectifying circuit with an impedance matching circuit (Fig. S15) for improved sensitivity and efficiency over a broad frequency range including the target 2.4-2.5 GHz. Further integration of the stretchable 3D asymmetric double-arched antenna with the flexible rectifier yields a stretchable rectenna to efficiently harvest the RF energy at Wi-Fi frequencies for over-the-air wireless power transmission. The harvested ambient RF energy is sufficient to power and light up a red light-emitting diode (LED) (APHB1608ZGKSURKC, 20 mA) (Fig. 6e and Movie S2), which could possibly be used for wireless wound healing [47] or optogenetics [48]. The commercial temperature sensor (AS6212, AMS) can be also powered by the harvested RF energy, with the sensing data wirelessly transmitted to a smartphone in real time through low-power Bluetooth for display and easy readout (Fig. S16 and Movie S3). To further demonstrate the feasibility of an integrated standalone stretchable RF system, we combine the stretchable rectenna with stretchable sensing and energy storage modules for a self-powered stretchable system. In a proof-of-the-concept demonstration (Fig. 7a), the stretchable rectenna based on the "Asy 1:2" microstrip antenna is integrated with a flexible supercapacitor (Fig. S17a, c) and a stretchable strain sensor (Fig. S17b,

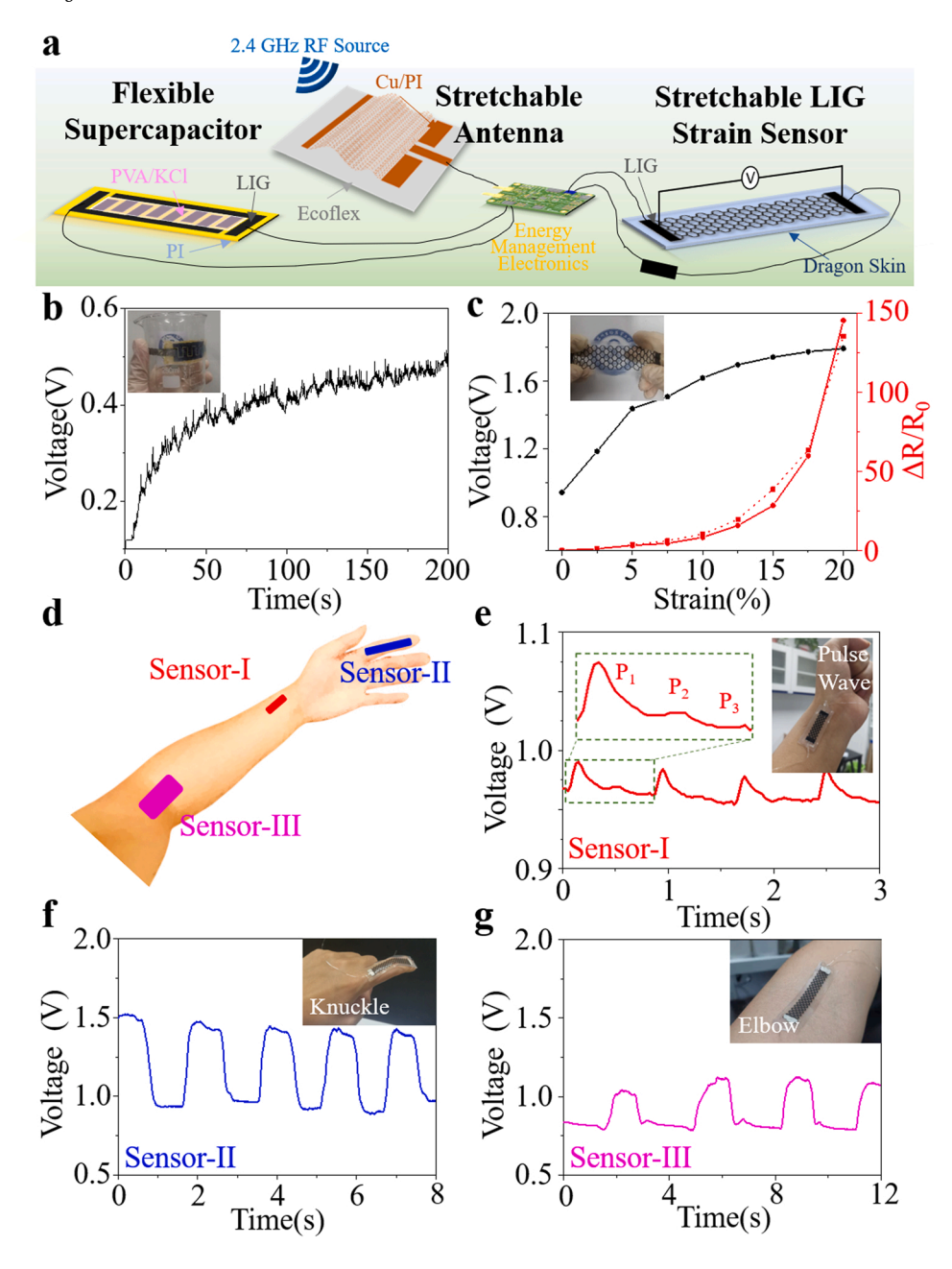


Fig. 7. Integrated standalone stretchable RF systems. (a) Schematic diagram of integrated standalone stretchable RF systems, which include the stretchable rectenna based on the "Asy_1:2" microstrip antenna, a flexible supercapacitor and a stretchable strain sensor. (b) Charging curve of the LIG-based flexible supercapacitor. (c) The direct electromechanical characterization (dashed) and corresponding voltage measurement (solid black) and derived resistance change (solid red) in a series circuit powered by the integrated rectenna as a function of the applied tensile strain. (d) Schematic showing the positions of three RFpowered LIG strain sensors for monitoring (e) pulse wave, (f) knuckle motion, and (g) elbow

d), both based on laser-induced graphene (LIG) foam. In such a system, the flexible supercapacitor is efficiently charged by the stretchable rectenna, which only takes ~ 200 s to go from 0 to 0.5 V (Fig. 7b). The stored energy in the supercapacitor can generate a constant output voltage of ~1.8 V to power the LIG-based stretchable strain sensor. Electromechanical measurements of the LIG-based strain sensor exhibit a J-shaped curve in the relative resistance change as a function of the applied strain up to 20% (Fig. 7c). By connecting the LIG-based strain sensor to a resistor with a known resistance in series subject to the constant output voltage of the rectifying circuit, the applied strain can be obtained from the measured voltage across the strain sensor (Fig. S18 and Movie S4). The stretchable RF-powered LIG strain sensor can also be applied to the human body for healthcare monitoring and human motion detection (Fig. 7d, Fig. S19, and Movie S5). The sensor attached to the wrist provides continuous and wireless monitoring of pulse waveform from the radial artery (Fig. 7e), whereas the ones on the knuckle and elbow allow the real-time motion detection of the finger (Fig. 7 f) and elbow (Fig. 7 g). The results pave the way for the future integrated

standalone stretchable RF systems with wireless communication capabilities and sustained power supplies for long-term, convenient, and continuous monitoring of human and structural health.

Supplementary material related to this article can be found online at.

3. Conclusion

In summary, the stretchable 3D double-arched microstrip antennas have been designed, fabricated, and characterized. The measurements of the coupled mechanical-electromagnetic property demonstrate that the 3D double-arched microstrip antennas exhibit strain-insensitive resonance, improved stretchability, and enhanced peak gain compared with their 2D counterpart. In particular, the enhanced peak gain of the stretchable 3D microstrip antennas from the reduced effective dielectric constant contributes to drastically improved on-body wireless communication and RF energy harvesting performance. Specifically, the excellent on-body radiation performance of the stretchable 3D microstrip antenna features a longer communication distance, lower package

loss rate, higher RF energy harvesting level. The harvested RF energy is also sufficient to power a LED or wireless temperature sensing. The comparison between the symmetric and asymmetric 3D structures also reveals the high potential of exploring 3D antennas with different configurations for further optimization in on-body performance. More importantly, the integration of wireless transmission and RF energy harvesting modules with stretchable sensors and energy storage units such as micro-supercapacitors provide the proof-of-the-concept demonstration of a standalone stretchable RF system. The integrated self-powered stretchable system with wireless capabilities paves the way for future health monitoring of humans and structures. The demonstrated results also open up new opportunities in self-powered sensing notes for soft body area networks or smart internet-of-things.

4. Experimental section

4.1. Fabrication of 3D symmetric or asymmetric arched microstrip antennas

The fabrication of 3D double-arched microstrip antennas began with patterning of the meshed patch and ground plane on copper foils by an ultraviolet laser (LPKF Laser U4, power: 0.4 μJ ; speed: 2000 mm s $^{-1}$; wavelength: 355 nm). A silicone substrate (Ecoflex 00–30) with a thickness of 1.5 mm was prepared by mixing the precursor solution (Part A and B) with a ratio of 1:1, degassing in a vacuum, and then curing at room temperature. The meshed ground was then fully bonded to a prestretched silicone substrate by silicone glue. The meshed patch was then selectively bonded on the other side of the silicone substrate at predefined bonding sites. The release of pre-strain generated wrinkled structure in the meshed ground and 3D arches in the patch. The difference in the selective bonding sites resulted in three representative double-arched structures: symmetric ("Sym_1:1") or asymmetric ("Asy_1:2" and "Asy_2:1") patches.

4.2. Finite element analysis (FEA) of double-arched patches

The mechanical deformation and strain distribution in the asymmetric and symmetric double-arched patches were obtained by FEA implemented in ABAQUS (6.13, ABAQUS Inc.). A shell model with a thickness of 10 μ m was chosen for the thin patch in the simulation. The elastic modulus and Poisson's ratio of Cu were set as 119 GPa and 0.34, respectively.

4.3. Measurement of S_{11} curves and radiation patterns of the stretchable microstrip antenna

The mechanical-electromagnetic properties of the 2D and 3D stretchable microstrip antennas being stretched by a custom-built stretcher were measured by a network analyzer (T5260A, Transcom Instruments) with the open-short-load-through calibration. After connecting the antenna soldered with a SubMiniature version A (SMA) connector to the instrument with a coaxial cable, the reflection curves (S₁₁) were simultaneously recorded by this instrument as the antenna was stretched to different strain levels. The radiation patterns of the stretchable microstrip antenna before and after stretching were measured in an anechoic chamber with a directional horn antenna as the receiver for every angular position. The on-body performance of the antenna was measured by attaching it to the arm of a healthy human subject with a thin adhesive Silbione layer.

4.4. Evaluation of on-body wireless communication and RF energy harvesting performance

The wireless communication performance of the stretchable microstrip antennas was evaluated by a commercial RF evaluation kit (SmartRF06, Texas Instruments). A wireless communication module

(CC2538EMK, Texas Instruments) in a transmitter that integrated with the stretchable microstrip antenna was programmed to transmit RF energy at a power of -3 dBm. A receiver board with the same chip (sensitivity of -100 dB) was used to communicate with the transmitter. The received energy and packet loss rate were measured by placing the receiver from the transmitter at different distances.

The RF energy harvesting performance of the stretchable microstrip antenna was measured by connecting it with a commercial RF energy harvesting evaluation kit (AEM30940 2.45 GHz EVK, e-peas). The same RF module used in wireless communication was explored to transmit the RF energy at a power of 7 dBm. An electrochemical station was used to measure the open-circuit voltage of the farad capacitor and flexible supercapacitor charged by the rectenna based on the 3D microstrip antennas ("Sym_1:1" or "Asy_1:2") and their 2D counterpart in real-time with a sampling rate of 10 Hz.

4.5. Fabrication of the flexible rectifier circuit

The fabrication of the flexible rectifier circuit began with patterning of the circuit pattern and ground plane on copper foils by an ultraviolet laser (LPKF Laser U4, power: $0.4~\mu J$; speed: $2000~mm~s^{-1}$; wavelength: 355~nm). A silicone substrate (Ecoflex $00{\text -}30$) with a thickness of 1.5~mm and through-hole was prepared by mixing the precursor solution (Part A and B) with a ratio of 1:1, degassing in a vacuum, and then pouring into the mold and curing at room temperature. The circuit pattern was then fully bonded to the Ecoflex substrate by silicone glue, and the ground plane was then bonded on the other side of the substrate, then the silver silk was used for connecting the them at the location of through-hole. Finally, electrical component could be reliably soldered on the Cu circuit using conventional solder paste (Sn42Bi58, KZ-1513) according to the layout file.

4.6. Fabrication of the LIG-based flexible supercapacitor and stretchable strain sensor

The fabrication of the LIG-based flexible supercapacitor began with patterning of the PI sheets by a $\rm CO_2$ laser (VLS 3.50, Universal) in the raster mode (Power: 8.0%, Speed: 15%). Next, the gel electrolyte was prepared by adding 6 g KCl and 12 g poly(vinyl alcohol) (PVA) into 100 mL deionized water, followed by magnetic stirring at 85 °C for 1 h. The solution was drop-coated onto the LIG interdigitated electrode and dried in air at 25 °C for 5 h. The fabrication of the LIG-based strain sensor followed the same scribing process. Next, a silicone precursor (Dragon Skin 00–30, the weight ratio of part A: part B = 1:1) was drop-coated onto the LIG. After curing, the silicone substrate was manually peeled off from the PI film to yield the stretchable LIG-based strain sensor

CRediT authorship contribution statement

Zhang Senhao: Conceptualization, Methodology, Validation, Formal analysis, Investigation, Data curation, Writing - original draft, Writing - review & editing, Visualization. Zhu Jia: Conceptualization, Methodology, Formal analysis, Investigation, Writing - original draft, Writing - review & editing, Visualization, Supervision, Project administration. Zhang Yingying: Software, Formal analysis, Investigation, Resources. Chen Zhensheng: Methodology, Data curation. Song Chaoyun: Methodology, Data curation. Li Jiuqiang: Formal analysis, Methodology. Yi Ning: Software. Qiu Donghai: Software. Guo Kai: Data curation. Zhang Cheng: Validation. Validation. Pan Tailong: Validation. Zhou Honglei:Lin Yuan: Software. Long Hao: Software. Yang Hongbo: Conceptualization, Methodology, Validation, Writing original draft, Writing - review & editing, Project administration, Funding acquisition. Cheng Huanyu Conceptualization, Methodology, Validation, Writing - original draft, Writing - review & editing, Visualization, Supervision, Project administration, Funding acquisition.

Declaration of Competing Interest

The authors declare that they have no known competing financial interests or personal relationships that could have appeared to influence the work reported in this paper.

Acknowledgments

H.Y. acknowledges the supports provided by the International Partnership Program of the Chinese Academy of Science (Grant no. 154232KYSB20200016), the National Key Research and Development Program of China (Grant no. 2020YFC2007400), and the Key Research and Development Program of Jiangsu Province (Grant no. BE2021012-1). H.C. acknowledges the supports provided by the National Science Foundation (NSF) (Grant no. ECCS-1933072), the National Heart, Lung, and Blood Institute of the National Institutes of Health under Award no. R61HL154215, the National Institute of Biomedical Imaging and Bioengineering of the National Institutes of Health under Award no. R21EB030140 and Penn State University. The partial support from various Penn State Seed Grants provided by the Center for Biodevices, the College of Engineering, and the Center for Security Research and Education is also acknowledged. S.Z. would like to acknowledge Qi Lu's love and parents' support, as well as the help from Jingxin Lu, Benkun Bao, Han Wu, Dr. Kong on the wireless communication measurement and ambient RF energy harvesting. J.Z. would like to acknowledge the Leighton Riess Graduate Fellowship and Diefenderfer Graduate Fellowship in Engineering at Penn State University.

Appendix A. Supporting information

Supplementary data associated with this article can be found in the online version at doi:10.1016/j.nanoen.2022.107069.

References

- Z. Xie, R. Avila, Y. Huang, J.A. Rogers, Flexible and stretchable antennas for biointegrated electronics, Adv. Mater. 32 (2020) 1902767, https://doi.org/ 10.1002/edws.201002767
- [2] K. Yamagishi, W. Zhou, T. Ching, S.Y. Huang, M. Hashimoto, Ultra-deformable and tissue-adhesive liquid metal antennas with high wireless powering efficiency, Adv. Mater. 33 (2021) 2008062, https://doi.org/10.1002/adma.202008062.
- [3] J. Zhu, H. Cheng, Recent development of flexible and stretchable antennas for biointegrated electronics, Sensors 18 (2018), 124364, https://doi.org/10.3390/ s18124364
- [4] H.U. Chung, B.H. Kim, J.Y. Lee, J. Lee, Z. Xie, E.M. Ibler, K. Lee, A. Banks, J. Y. Jeong, J. Kim, C. Ogle, D. Grande, Y. Yu, H. Jang, P. Assem, D. Ryu, J.W. Kwak, M. Namkoong, J.B. Park, Y. Lee, D.H. Kim, A. Ryu, J. Jeong, K. You, B. Ji, Z. Liu, Q. Huo, X. Feng, Y. Deng, Y. Xu, K.I. Jang, J. Kim, Y. Zhang, R. Ghaffari, C.M. Rand, M. Schau, A. Hamvas, D.E. Weese-Mayer, Y. Huang, S.M. Lee, C.H. Lee, N. R. Shanbhag, A.S. Paller, S. Xu, J.A. Rogers, Binodal, wireless epidermal electronic systems with in-sensor analytics for neonatal intensive care, Science 363 (2019) 6430, https://doi.org/10.1126/science.aau0780.
- [5] M. Mahmood, D. Mzurikwao, Y.-S. Kim, Y. Lee, S. Mishra, R. Herbert, A. Duarte, C. S. Ang, W.-H. Yeo, Fully portable and wireless universal brain–machine interfaces enabled by flexible scalp electronics and deep learning algorithm, Nat. Mach. Intell. 1 (2019) 412–422, https://doi.org/10.1038/s42256-019-0091-7.
- [6] J. Kim, A. Banks, H. Cheng, Z. Xie, S. Xu, K.I. Jang, J.W. Lee, Z. Liu, P. Gutruf, X. Huang, P. Wei, F. Liu, K. Li, M. Dalal, R. Ghaffari, X. Feng, Y. Huang, S. Gupta, U. Paik, J.A. Rogers, Epidermal electronics with advanced capabilities in near-field communication, Small 11 (2015) 906–912, https://doi.org/10.1002/smll.201402495.
- [7] K. Pan, Y. Fan, T. Leng, J. Li, Z. Xin, J. Zhang, L. Hao, J. Gallop, K.S. Novoselov, Z. Hu, Sustainable production of highly conductive multilayer graphene ink for wireless connectivity and IoT applications, Nat. Commun. 9 (2018) 5197, https://doi.org/10.1038/s41467-018-07632-w.
- [8] X. Tian, P.M. Lee, Y.J. Tan, T.L.Y. Wu, H. Yao, M. Zhang, Z. Li, K.A. Ng, B.C.K. Tee, J.S. Ho, Wireless body sensor networks based on metamaterial textiles, Nat. Electron. 2 (2019) 243–251, https://doi.org/10.1038/s41928-019-0257-7.
- [9] C. Zhang, Z. Peng, C. Huang, B. Zhang, C. Xing, H. Chen, H. Cheng, J. Wang, S. Tang, High-energy all-in-one stretchable micro-supercapacitor arrays based on 3D laser-induced graphene foams decorated with mesoporous ZnP nanosheets for self-powered stretchable systems, Nano Energy 81 (2021), 105609, https://doi. org/10.1016/j.nanoen.2020.105609.
- [10] C. Zhang, H. Chen, X. Ding, F. Lorestani, C. Huang, B. Zhang, B. Zheng, J. Wang, H. Cheng, Y. Xu, Human motion-driven self-powered stretchable sensing platform

- based on laser-induced graphene foams, Appl. Phys. Rev. 9 (2022), 011413, https://doi.org/10.1063/5.0077667.
- [11] Z. Chen, J. Xi, W. Huang, M.M.F. Yuen, Stretchable conductive elastomer for wireless wearable communication applications, Sci. Rep. 7 (2017) 10958, https://doi.org/10.1038/s41598-017-11392-w.
- [12] S. Choi, H. Lee, R. Ghaffari, T. Hyeon, D.H. Kim, Recent advances in flexible and stretchable bio-electronic devices integrated with nanomaterials, Adv. Mater. 28 (2016) 4203–4218, https://doi.org/10.1002/adma.201504150.
- [13] Y. Ma, Y. Zhang, S. Cai, Z. Han, X. Liu, F. Wang, Y. Cao, Z. Wang, H. Li, Y. Chen, X. Feng, Flexible hybrid electronics for digital healthcare, Adv. Mater. 32 (2020) 1902062, https://doi.org/10.1002/adma.201902062.
- [14] Y. Lin, J. Genzer, M.D. Dickey, Attributes, fabrication, and applications of gallium-based liquid metal particles, Adv. Sci. 7 (2020) 2000192, https://doi.org/10.1002/advs.202000192.
- [15] G. Xu, L. Yuan, X. Chen, W. Jia, M. Wang, L. Yang, J. Zhu, H. Cheng, Design of non-dimensional parameters in stretchable microstrip antennas with coupled mechanics-electromagnetics, Mater. Des. 205 (2021), 109721, https://doi.org/10.1016/j.matdes.2021.109721.
- [16] L. Song, A.C. Myers, J.J. Adams, Y. Zhu, Stretchable and reversibly deformable radio frequency antennas based on silver nanowires, ACS Appl. Mater. Interfaces 6 (2014) 4248–4253, https://doi.org/10.1021/am405972e.
- [17] F. Nikbakhtnasrabadi, H. El Matbouly, M. Ntagios, R. Dahiya, Textile-based stretchable microstrip antenna with intrinsic strain sensing, ACS Appl. Electron. Mater. 3 (2021) 2233–2246, https://doi.org/10.1021/acsaelm.1c00179.
- [18] J. Zhu, J.J. Fox, N. Yi, H. Cheng, Structural design for stretchable microstrip antennas, ACS Appl. Mater. Interfaces 11 (2019) 8867–8877, https://doi.org/ 10.1021/acsami.8b22021.
- [19] Y.R. Jeong, J. Kim, Z. Xie, Y. Xue, S.M. Won, G. Lee, S.W. Jin, S.Y. Hong, X. Feng, Y. Huang, J.A. Rogers, J.S. Ha, A skin-attachable, stretchable integrated system based on liquid GalnSn for wireless human motion monitoring with multi-site sensing capabilities, NPG Asia Mater. 9 (2017), e443, https://doi.org/10.1038/am.2017.189.
- [20] Y. Li, X. Tian, S.P. Gao, L. Jing, K. Li, H. Yang, F. Fu, J.Y. Lee, Y.X. Guo, J.S. Ho, P. Y. Chen, Reversible crumpling of 2D titanium carbide (MXene) nanocoatings for stretchable electromagnetic shielding and wearable wireless communication, Adv. Funct. Mater. 30 (2019) 1907451, https://doi.org/10.1002/adfm.201907451.
- [21] J.-H. So, J. Thelen, A. Qusba, G.J. Hayes, G. Lazzi, M.D. Dickey, Reversibly deformable and mechanically tunable fluidic antennas, Adv. Funct. Mater. 19 (2009) 3632–3637, https://doi.org/10.1002/adfm.200900604.
- [22] F.A. Tahir, A. Javed, A compact dual-band frequency-reconfigurable textile antenna for wearable applications, Microw. Opt. Technol. Lett. 57 (2015) 2251–2257, https://doi.org/10.1002/mop.29311.
- [23] R. Sharma, R. Mishra, T. Ngo, Y.X. Guo, S. Fukami, H. Sato, H. Ohno, H. Yang, Electrically connected spin-torque oscillators array for 2.4 GHz WiFi band transmission and energy harvesting, Nat. Commun. 12 (2021) 2924, https://doi. org/10.1038/s41467-021-23181-1.
- [24] V. Vallem, Y. Sargolzaeiaval, M. Ozturk, Y.C. Lai, M.D. Dickey, Energy harvesting and storage with soft and stretchable materials, Adv. Mater. 33 (2021) 2004832, https://doi.org/10.1002/adma.202004832.
- [25] M.R. Elhebeary, M.A.A. Ibrahim, M.M. Aboudina, A.N. Mohieldin, Dual-source self-start high-efficiency microscale smart energy harvesting system for IoT, IEEE Trans. Ind. Electron. 65 (2018) 342–351, https://doi.org/10.1109/tje.2017.2714119
- [26] P. He, M.S. Cao, W.Q. Cao, J. Yuan, Developing mxenes from wireless communication to electromagnetic attenuation, Nano Micro Lett. 13 (2021) 115, https://doi.org/10.1007/s40820-021-00645-z.
- [27] Y. Hu, T. Zhao, P. Zhu, Y. Zhu, X. Shuai, X. Liang, R. Sun, D.D. Lu, C.-P. Wong, Low cost and highly conductive elastic composites for flexible and printable electronics, J. Mater. Chem. C 4 (2016) 5839–5848, https://doi.org/10.1039/C6TC01340F.
- [28] C. Mendes, C. Peixeiro, On-body transmission performance of a novel dual-mode wearable microstrip antenna, IEEE Trans. Antennas Propag. 66 (2018) 4872–4877, https://doi.org/10.1109/tap.2018.2851669.
- [29] J. Zhu, Z. Hu, C. Song, N. Yi, Z. Yu, Z. Liu, S. Liu, M. Wang, M.G. Dexheimer, J. Yang, H. Cheng, Stretchable wideband dipole antennas and rectennas for RF energy harvesting, Mater. Today Phys. 18 (2021), 100377, https://doi.org/ 10.1016/j.mtphys.2021.100377.
- [30] K.Y. Shin, J.Y. Hong, J. Jang, Micropatterning of graphene sheets by inkjet printing and its wideband dipole-antenna application, Adv. Mater. 23 (2011) 2113–2118, https://doi.org/10.1002/adma.201100345.
- [31] J. Zhu, S. Zhang, N. Yi, C. Song, D. Qiu, Z. Hu, B. Li, C. Xing, H. Yang, Q. Wang, H. Cheng, Strain-insensitive hierarchically structured stretchable microstrip antennas for robust wireless communication, Nano Micro Lett. 13 (2021) 108, https://doi.org/10.1007/s40820-021-00631-5.
- [32] Y.S. Kim, A. Basir, R. Herbert, J. Kim, H. Yoo, W.H. Yeo, Soft materials, stretchable mechanics, and optimized designs for body-wearable compliant antennas, ACS Appl. Mater. Interfaces 12 (2020) 3059–3067, https://doi.org/10.1021/ acsami.9b20233.
- [33] T. Rai, P. Dantes, B. Bahreyni, W.S. Kim, A stretchable RF antenna with silver nanowires, IEEE Electron. Device Lett. 34 (2013) 544–546, https://doi.org/ 10.1109/led.2013.2245626.
- [34] F. Nikbakhtnasrabadi, H. El Matbouly, M. Ntagios, R. Dahiya, Textile-based stretchable microstrip antenna with intrinsic strain sensing, ACS Appl. Electron. Mater. 3 (2021) 2233–2246, https://doi.org/10.1021/acsaelm.1c00179.
- [35] A. Michel, R. Colella, G.A. Casula, P. Nepa, L. Catarinucci, G. Montisci,
 G. Mazzarella, G. Manara, Design considerations on the placement of a wearable

- UHF-RFID PIFA on a compact ground plane, IEEE Trans. Antennas Propag. 66 (2018) 3142–3147, https://doi.org/10.1109/tap.2018.2811863.
- [36] F. Xu, K. Zhang, Y. Qiu, Light-weight, high-gain three-dimensional textile structural composite antenna, Compos. B Eng. 185 (2020), 107781, https://doi. org/10.1016/j.compositesb.2020.107781.
- [37] K. Zhang, L. Zheng, F.I. Farha, L. Wang, F. Xu, Three-dimensional textile structural conical conformal microstrip antennas for multifunctional flexible electronics, ACS Appl. Electron. Mater. 2 (2020) 1440–1448, https://doi.org/10.1021/ acsaelm 0c00200
- [38] M.T. Ali, H. Jaafar, S. Subahir, A.L. Yusof, Gain enhancement of air substrates at 5.8GHz for microstrip antenna array, IEEE APEMC (2012) 477–480, https://doi. org/10.1109/APEMC.2012.6237872.
- [39] S.B. Yeap, Z.N. Chen, Microstrip patch antennas with enhanced gain by partial substrate removal, IEEE Trans. Antennas Propag. 58 (2010) 2811–2816, https:// doi.org/10.1109/TAP.2010.2052572.
- [40] Z. Yan, F. Zhang, F. Liu, M. Han, D. Ou, Y. Liu, Q. Lin, X. Guo, H. Fu, Z. Xie, M. Gao, Y. Huang, J. Kim, Y. Qiu, K. Nan, J. Kim, P. Gutruf, H. Luo, A. Zhao, K.-C. Hwang, Y. Huang, Y. Zhang, J.A. Rogers, Mechanical assembly of complex, 3D mesostructures from releasable multilayers of advanced materials, Sci. Adv. 2 (2016) 1601014, https://doi.org/10.1126/sciadv.1601014.
- [41] S. Zhang, W. Whittow, R. Seager, A. Chauraya, J.C. Vardaxoglou, Non-uniform mesh for embroidered microstrip antennas, IET Microw. Antennas Propag. 11 (2017) 1086–1091, https://doi.org/10.1049/iet-map.2016.0901.
- [42] A.S. Mekki, M.N. Hamidon, A. Ismail, A.R.H. Alhawari, Gain enhancement of a microstrip patch antenna using a reflecting layer, Int. J. Antennas Propag. 2015 (2015), 975263, https://doi.org/10.1155/2015/975263.
- [43] A.P. Ghodake, H.B. Sale, 2018. Gain Enhancement of Microstrip Antenna, IEEE. ICACAT., 1–6, http://doi.org/10.1109/ICACAT.2018.8933621.
- [44] G. Clasen, R. Langley, Meshed patch antennas, IEEE Trans. Antennas Propag. 52 (2004) 1412–1416, https://doi.org/10.1109/tap.2004.830251.
- [45] T. Chang, Y. Tanabe, C.C. Wojcik, A.C. Barksdale, S. Doshay, Z. Dong, H. Liu, M. Zhang, Y. Chen, Y. Su, T.H. Lee, J.S. Ho, J.A. Fan, A general strategy for stretchable microwave antenna systems using serpentine mesh layouts, Adv. Funct. Mater. 27 (2017) 1703059, https://doi.org/10.1002/adfm.201703059.
- [46] C. Song, P. Lu, S. Shen, Highly efficient omnidirectional integrated multiband wireless energy harvesters for compact sensor nodes of internet-of-things, IEEE Trans. Ind. Electron. 68 (2021) 8128–8140, https://doi.org/10.1109/ TIE.2020.3009586.
- [47] M.E. Chaves, A.R. Araújo, A.C. Piancastelli, M. Pinotti, Effects of low-power light therapy on wound healing: LASER x LED, An. Bras. Dermatol. 89 (2014) 616–623, https://doi.org/10.1590/abd1806-4841.20142519.
- [48] M.A. Rossi, V. Go, T. Murphy, Q. Fu, J. Morizio, H.H. Yin, A wirelessly controlled implantable LED system for deep brain optogenetic stimulation, Front. Integr. Neurosci. 9 (2015) 8, https://doi.org/10.3389/fnint.2015.00008.



Senhao Zhang received a B.E. degree in Mechanical and Electronic Engineering from Soochow University, Suzhou, China, in 2017. He is currently pursuing the Ph.D. degree at the University of Science and Technology of China. His current research interests include Wearable skin-like sensors, Antennas, Rectifying antennas, Lu Qi's happiness, and RF energy harvesting.



Jia Zhu earned a Ph.D. degree from the Pennsylvania State University in 2019. He works as a post-doctor at Dr. Huanyu Cheng's research group. Jia Zhu is working on the design of various flexible/stretchable sensors, RF devices, and integrated systems for human health monitoring. He has received several fellowships from the engineering school at The Pennsylvania State University and NSF.



Yingying Zhang was born in Heilongjiang, China, in 1993. She received the B.S. degrees from the school of mechanical engineering, Ji Lin University, China, in 2015 and M.S. degrees from the school of mechanical engineering, University of Chinese Academy of Sciences, China, in 2018. From 2018, she worked in the Suzhou Institute of Biomedical Engineering Technology, Chinese Academy of Sciences, engaged in the research of Flexible electronics. She is now a research assistant.



Zhensheng Chen received the B.E. degree and the M.Sc. degree (Hons.) in communication engineering from Lanzhou University, Lanzhou, China, in 2015, and 2018, respectively. He is currently pursuing the Ph.D. degree at KU Leuven, Belgium. His current research interests include wearable antennas, rectifying antennas, wireless power transfer, and RF energy harvesting.



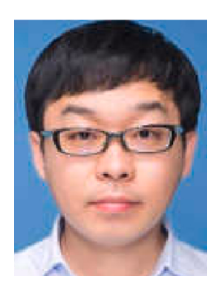
Prof. Chaoyun Song received BEng. MSc and Ph.D. degrees in electrical engineering and electronics from The University of Liverpool, Liverpool, UK. He is currently an Assistant Professor with the School of Engineering and Physical Sciences (EPS), Heriot-Watt University, Edinburgh, Scotland, UK. He has published more than 70 papers in peer-reviewed journals and conference proceedings. His current research interests include wireless energy harvesting and wireless power transfer technologies, antennas and microwave circuits, metamaterials and meta-surfaces in RF, energy harvesting and sensing technologies.



Jiuqiang Li was born in Zhejiang, China, in 1997. He received the B.S. degree from the School of Logistics Engineering, Wuhan University of Technology, China, in 2019. From 2020, he has studied in the Suzhou Institute of Biomedical Engineering and Technology, Chinese Academy of Sciences for the M.S. degree and engaged in the research of skin-like sensors.



Ning Yi received his bachelor's degree from the department of materials science and engineering from Pennsylvania State University in 2014. After the graduation from materials science and engineering department at Penn State, he started as a Ph.D. student in the department of biomedical engineering. In 2015, he transferred back to the department of materials science and engineering and joined Prof. Huanyu Cheng's lab. His research interests include stretchable gas sensors, transient epidermal sensors, and novel fabrication methods for constructing electronics on curvilinear surfaces. Currently, Ning has coauthored 9 peer-reviewed publications.



Donghai Qiu was born in Zhejiang, China, in 1988. He received the double PhD degrees from the Institut National des Sciences Appliquées and Chinese Academy of Sciences in France and in China, respectively. From 2018, he worked in the Suzhou Institute of Biomedical Engineering Technology, Chinese Academy of Sciences, engaged in the research of rehabilitation engineering, flexible electronics and vital signs detection technology. He is now an Associate Research Fellow.



Honglei Zhou is a postdoctoral fellow in the Department of Engineering Mechanics at Tsinghua University, Beijing, China, and Institute of Flexible Electronics Technology of THU, Jiaxing, China. Received the M.S.E. and Ph.D. degree in Department of Engineering Mechanics from Northwestern Polytechnical University, Xi'an, China. His research interests include mechanics of stretchable and flexible electronics, piezoelectric vibration energy harvester, piezoelectric ultrasonic transducer, and ultrasound medical devices.



Kai Guo was born in Anhui, China, in 1993. He received the B. S. and M.S. degrees from the School of Mechatronics Engineering, Harbin Institute of Technology, China, in 2013 and 2015, respectively. From 2015, he worked in the Suzhou Institute of Biomedical Engineering Technology, Chinese Academy of Sciences, engaged in the research of rehabilitation robots and surgical robots. He is now an Associate Research Fellow and a master's supervisor.



Hao Long was born in Guizhou, China, in 1997. He received the B.E. degree in electronic information engineering from Soochow University, Suzhou, China, in 2021, where he is currently pursuing the M.E. degree in electronic and communication engineering.



Cheng Zhang received a B.S. degree from the Department of Physics, Huanggang Normal University, China, in 2010. He received a Ph.D. degree from Nanjing University in 2018. He is now an assistant professor at Minjiang University, China. His research interests include the synthesis, fabrication, and assembly of inorganic materials for energy and environmental applications.



Prof. Hongbo Yang presided over and participated in the completion of a number of national, Chinese Academy of Sciences and provincial and ministerial projects. He is currently the director of the Rehabilitation Engineering Technology Research Laboratory of Suzhou Institute of biomedical engineering technology, Chinese Academy of Sciences and Suzhou Key Laboratory of rehabilitation engineering, and the distinguished researchers of Chinese Academy of Sciences. His current research interests include wearable Skin-like Sensor, Antennas, RF energy harvesting and Rehabilitation engineering technology.



Taisong Pan received his Ph.D. degree from University of Electronic Science and Technology of China in 2016. He is currently an associate professor in the School of Materials and Energy at University of Electronic Science and Technology of China. His research interests include flexible/stretchable sensors, reconfigurable electronic devices and deformable microwave components.



Prof. Huanyu Cheng earned a Ph.D. degree from Northwestern University in 2015 and a Bachelor's degree from Singhua University in 2010. After his doctoral study, he was appointed as the Dorothy Quiggle Assistant Professor of Engineering Science and Mechanics at The Pennsylvania State University. Dr. Cheng has worked on standalone stretchable sensing systems for biomedicine with over 100 peer-reviewed publications, and his work has been recognized through the reception of numerous awards. He also serves as an associate editor for IEEE Internet of Things Journal, Computers in Biology and Medicine, and reviewer for over 180 international iournals.



Yuan Lin received her Ph.D. degree from University of Science and Technology of China in 1999. She is currently a professor in the School of Materials and Energy at University of Electronic Science and Technology of China. Her main research interests are in the development of inorganic functional materials for applications in stretchable and flexible electronics.